

CALL FOR PAPERS | *Bioengineering the Lung: Molecules, Materials, Matrix, Morphology, and Mechanics*

Fibroblast engraftment in the decellularized mouse lung occurs via a β 1-integrin-dependent, FAK-dependent pathway that is mediated by ERK and opposed by AKT

Huanxing Sun,¹ Elizabeth Calle,² Xiaosong Chen,^{1,3} Aditi Mathur,¹ Yangyang Zhu,^{1,3} Julio Mendez,² Liping Zhao,² Laura Niklason,² Xueyan Peng,¹ Hong Peng,^{1,5} and Erica L. Herzog¹

¹Departments of Internal Medicine, Section of Pulmonary, Critical Care, and Sleep Medicine and ²Anesthesiology, Yale School of Medicine, New Haven; ³Beijing University of Chinese Medicine, Second School of Clinical Chinese Medicine, Beijing; ⁴School of Engineering, University of Connecticut, Farmington, Connecticut; and ⁵The Second Xiangya Hospital of Central-South University, Department of Respiratory Medicine, Changsha, Hunan, China

Submitted 17 April 2013; accepted in final form 2 December 2013

Sun H, Calle E, Chen X, Mathur A, Zhu Y, Mendez J, Zhao L, Niklason L, Peng X, Peng H, Herzog EL. Fibroblast engraftment in the decellularized mouse lung occurs via a β 1-integrin-dependent, FAK-dependent pathway that is mediated by ERK and opposed by Akt. *Am J Physiol Lung Cell Mol Physiol* 306: L463–L475, 2014. First published December 13, 2013; doi:10.1152/ajplung.00100.2013.—Creation of bioartificial organs has been enhanced by the development of strategies involving decellularized mammalian lung. Because fibroblasts critically support lung function through a number of mechanisms, study of these cells in the context of the decellularized lung has the potential to improve the structure and function of tissue-engineered lungs. We characterized the engraftment and survival of a mouse fibroblast cell line in decellularized rat lung slices and found a time-dependent increase in cell numbers assessed by hematoxylin and eosin staining, cell proliferation assessed by Ki67 staining, and minimal cell death assessed by TUNEL staining. We developed a repopulation index to allow quantification of cell survival that accounts for variation in cell density throughout the seeded scaffold. We then applied this method to the study of mouse lung scaffolds and found that decellularization of presliced mouse lungs produced matrices with preserved alveolar architecture and proteinaceous components including fibronectin, collagens I and IV, laminin, and elastin. Treatment with a β 1-integrin-neutralizing antibody significantly reduced the repopulation index after 24 h of culture. Treatment with focal adhesion kinase (FAK) inhibitor and extracellular signal-regulated kinase (ERK) inhibitor further reduced initial repopulation scores while treatment with AKT inhibitor increased initial scores. Rho-associated kinase inhibitor had no discernible effect. These data indicate that initial adhesion and survival of mouse fibroblasts in the decellularized mouse lung occur in a β 1-integrin-dependent, FAK/ERK-dependent manner that is opposed by AKT.

bioengineering; decellularized lung; fibroblast

EX VIVO ENGINEERING STRATEGIES have emerged as important approaches for the study of tissue regeneration in a wide variety of organs including the vasculature (20), genitourinary

Address for reprint requests and other correspondence: E. L. Herzog, Yale School of Medicine, Section of Pulmonary, Critical Care, and Sleep Medicine, 300 Cedar St. TAC 441S, New Haven CT 06520-8057 (e-mail: erica.herzog@yale.edu).

system (7), spinal cord (34), and kidney (28). Until recently, similar advances in pulmonary biology had been limited by the complex three-dimensional structure and functional anatomy of the intact lung. However, several studies describing the creation of functional tissue derived from existing (18) or fabricated airways (16, 18) or decellularized whole lungs (19, 23) have allowed major advances in the field of lung regeneration. For example, engineered human tracheas based on cadaverous (18) or synthetic (16) scaffolds have been used successfully to support the growth of airway cells and were later implanted into patients with tracheal anomalies. Similarly, decellularized rodent lungs have been used as a platform for the ex vivo regeneration of functional lung tissue that was suitable for in vivo implantation and mediated the transfer of oxygen from the alveolus into the pulmonary vasculature (19, 23). Analogous decellularization approaches applied to freshly resected or cadaverous human (2, 27) and mouse lungs (6) demonstrate this strategy to support the growth of epithelium and endothelium and even certain populations of stem cells.

The ultimate goal of this work involves the creation of bioengineered lungs built with autologous induced pluripotent stem cells, various populations of lung-specific progenitor cells, or perhaps even embryonic stem cells. All of these approaches will require a healthy extracellular matrix (ECM) to provide structural support (33). However, in the consideration of the long-term therapeutic application of scaffold-based strategies, several limitations become apparent. First, previous studies indicate that, even in the setting of grossly preserved structure and extracellular components, the decellularized lung scaffold demonstrates a large amount of “leakiness” that may at least partially reflect damage sustained during the decellularization procedure (12, 23). Second, other studies demonstrate that the decellularization process can negatively impact ECM protein integrity (1, 31), which may impede its ability to support infused progenitor cells or to persist long term in vivo. Thus studies aimed at restoring mesenchymal cells, such as fibroblasts that repair and maintain the structure and biochemical components of the decellularized ECM, have the potential to advance lung regeneration. Furthermore, once the bioengi-

neered lung is constructed and implanted, fibroblasts will be required to maintain ECM integrity in the steady state and to enact repair and remodeling in the setting of injury, as they are in the intact lung (3, 9, 25). However, if the goal is building patient-specific lungs using autologous cells, use of patient-specific lung fibroblasts may not be possible because obtaining sufficient numbers to build an entire organ would be prohibitive. Thus an alternate source of more easily obtainable fibroblasts, which could then be expanded *ex vivo*, such as dermal fibroblasts, might be more appropriate for this type of work.

Integrins are a large family of heterodimeric glycoprotein receptors that participate in important cellular processes, including ECM adhesion, cell:cell contact, transmembrane connections to the cytoskeleton, and activation of many intracellular signaling pathways (15). Among the integrin subunits, β 1-integrin is widely expressed and can bind multiple α -partners. β 1-Integrin importantly regulates the interaction between fibroblasts and ECM components, including certain collagens (30) and laminin (24). These effects are mediated in part by the activation of focal adhesion kinase (FAK) (30), a nonreceptor tyrosine kinase that upon engagement activates integral downstream signaling cascades, including extracellular-related kinase (ERK), Rho-associated kinase (ROCK), and phosphatidylinositol 3-kinase/AKT (6, 30). The β 1-integrin subunit is reported to mediate the initial interaction of mesenchymal stem cells and decellularized mouse lung scaffolds (6); however, the relationship of mature fibroblasts with the decellularized mouse lung and the involved signaling pathways have not been explored.

We sought to understand the kinetics and mechanism of dermal fibroblast engraftment in decellularized rodent lung scaffolds. We first determined that slices obtained from decellularized lung scaffolds prepared from rats, which are to date the only mammalian species that have been validated as a basis for the *ex vivo* regeneration of functional lung parenchyma, could support the adhesion, survival, and proliferation of a dermal fibroblast cell line. Next, to examine direct fibroblast-scaffold interactions and allow delineation of the engraftment mechanism(s) and to generate a method that would be useful in the study of human lung regeneration where starting material is scarce, we developed a decellularization system amenable for use on fresh mouse lung slices and characterized the cellular content and residual structural proteins in the resulting scaffolds. A9 dermal fibroblasts were then seeded into these scaffolds, and the kinetics of cell survival and expansion were defined. Last, the respective roles of β 1-integrin subunit and its downstream signaling partners FAK, ERK, ROCK, and AKT were assessed.

MATERIALS AND METHODS

Preparation of rat lung scaffold slices. All studies were performed with approval from the Yale University Institutional Animal Care and Use Committee. Rat lung harvest and decellularization were prepared as has been extensively described elsewhere (4, 21). Decellularized lungs were placed in a 60-mm sterile Petri dish that was then placed within a 100-mm Petri dish and floated on liquid nitrogen to snap freeze the scaffolds to facilitate precise slicing. Using sterile technique, scaffolds were cut into 2-mm slices by a multiknife and rinsed extensively with PBS containing 10% penicillin/streptomycin (Gibco, Grand Island, NY) and 2% gentamicin (Sigma-Aldrich, St. Louis, MO) for 1 h. Slices were stored at 4°C until the time of culture.

Preparation of mouse lung scaffold slices. Six- to twelve-week-old mice were treated with a lethal *i.p.* injection of Urethane (Sigma-Aldrich) and heparin (250 U/kg) (Sigma-Aldrich), followed by bronchoalveolar lavage and median thoractomy, and the pulmonary vasculature was perfused via right ventricular puncture with PBS. The lungs were removed *en bloc*, as we have previously described (26). Each lobe was placed in a 60-mm sterile Petri dish, which was transferred to a 100-mm Petri dish and floated on liquid nitrogen to snap freeze the lobes to allow precise slicing. With the use of a sterile technique, lobes were cut into about 2-mm slices by multiknife and rinsed extensively with PBS containing sodium nitroprusside at 1 μ g/ml for 1 h. The slices were transferred to a 15-ml tube and decellularized by 5 ml of decellularization solution [8 mM CHAPS (Sigma-Aldrich), 1 M NaCl, and 25 mM EDTA in PBS] per lung. The tube was kept at 37°C and rolled overnight. The scaffold slices were then extensively rinsed with PBS, treated with benzoylase nuclease (Sigma-Aldrich) (90 U/ml) for 1 h, and rinsed in PBS containing 10% penicillin/streptomycin and 2% gentamicin for 1 h. Prepared scaffold slices were stored in sterile PBS at 4°C until the time of culture.

Cell culture model and treatment. Mouse A9 cells (transformed subcutaneous fibroblasts) were cultured in DMEM (Gibco) supplemented with 5% fetal bovine serum (Gibco) and 1% penicillin/streptomycin and used before passage 40. Immediately before culture, lung scaffold slices were rinsed with PBS for 5 min, placed in a poly-L-lysine coated six-well plate (Becton Dickinson, Bedford, MA), extended with forceps, and incubated at 37°C for 10 min to allow adherence to the bottom of the plate. Then 1×10^4 , 1×10^5 , and 1×10^6 A9 cells in medium (100 μ l medium for rat slices and 50 μ l medium for mouse slices) were drizzled over the slice. The seeded slices were placed in the incubator for 30 min, at which point 1.7 ml (rat)/1.85 ml (mouse) of medium was added to the well. A quarter of medium volume was changed after 24 h and then every 48 h thereafter for a maximum culture period of 14 days.

Antibody-mediated β 1-integrin blockade. A9 cells were treated with a validated β 1-integrin-blocking antibody (Biolegend, San Diego, CA) or IgG isotype (Biolegend) (10) in a modification of previously published work (10). β 1-Integrin-blocking antibody (10 μ g/ml) or isotype was added to the resuspended cells and incubated at 4°C for 30 min. Cells (1×10^5) were then seeded on lung scaffold slices. Slices were collected after 24 h.

Chemical inhibition of FAK, ROCK, ERK, and AKT. For chemical treatment, FAK inhibitor 14 (Tocris Bioscience, Bristol, UK) (11), ROCK inhibitor (Calbiochem/EMD, Billerica, MA), ERK activation inhibitor (Tocris Bioscience), and AKT inhibitor VII/TAT-AKT-In (Calbiochem/EMD) (8) were added to the medium at the beginning of cell seeding. Cells (1×10^5) were seeded on lung scaffold slices. Slices were collected after 24 h.

Histological analysis. For histological evaluation, samples were fixed in 4% paraformaldehyde (Electron Microscopy Sciences, Hatfield, PA) for 2 to 4 h, dehydrated, embedded in paraffin, and sectioned at 5 μ m. Sections were stained with hematoxylin and eosin, Masson's Trichrome, Verheoff Van Gieson (VVG), and Alsace Blue to assess gross morphology, collagen fibers, elastin fibers, and glycosaminoglycans (GAGs), as we have previously described (23). Pictures were obtained using a Nikon microphot-fxa microscope.

Scanning electron microscopy. Samples were fixed using 4% glutaraldehyde (Electron Microscopy Sciences) in 0.1 M cacodylate buffer (Electron Microscopy Sciences) for 2 h at room temperature, then rinsed in cacodylate buffer, and dehydrated through an ethanol gradient. Samples were further dehydrated in Critical Point Dryer (Polaron E3000) by liquid CO₂, then sputter coated with gold, and analyzed using an ISI SS-40.

Immunofluorescence. Immunofluorescence detection of procollagen I α 1 (Rockland Immunohistochemicals, Rockland, MD), Ki67 (Abcam, Cambridge, MA), fibronectin (Abcam), collagen I (Rockland Immunohistochemicals), collagen IV (Abcam), and laminin (Abcam) were performed using antigen retrieval followed by secondary detec-

tion with Texas-Red-labeled secondary antibodies (Invitrogen, Eugene, OR), as well as 4', 6-diamidino-2-phenylindole (DAPI) (Vector Laboratories, Burlingame, CA) for DNA (21). End labeling of exposed 3'-OH ends of DNA fragments in paraffin-embedded tissue was undertaken with the TUNEL AP In Situ Cell Death Detection Kit (Roche Diagnostics, Mannheim, Germany) using the instructions provided by the manufacturer, as we have previously described (14). Microscopy was performed using a Nikon Eclipse Ti-S microscope equipped with a Andor Technology camera. Cell counting was performed manually. Quantification of mean fluorescence intensity was achieved using NIH Image J software.

Fluorometric DNA assay. DNA content of tissues was quantified using the Quant-iT PicoGreen dsDNA assay kit (Invitrogen), following manufacturer's instructions according to our previously published methods (23). Briefly, tissue samples were weighed and lyophilized, diluted in TE buffer, and mixed with the Quant-iT PicoGreen reagent. Fluorescence was measured at 520 nm with excitation at 485 nm, and DNA content was quantified using a standard curve.

Western blot. Successful elimination of cellular protein was confirmed by Western blot analysis of decellularized lung scaffold and normal mouse lung. The protein concentration was determined by the Pierce BCA protein assay kit (Pierce Biotechnology, Rockford, IL). Samples of 50 μ g of protein were loaded and separated by 10% SDS-PAGE and transferred to nitrocellulose membranes. After being blocked for 1 h at room temperature, the membranes were incubated with mouse anti-major histocompatibility complex (MHC II) polyclonal antibody (Abcam) or mouse anti- β -actin monoclonal antibody (Santa Cruz Biotechnology, Santa Cruz, CA) overnight at 4°C. The specific protein-antibody complex was detected by horseradish peroxidase-conjugated goat anti-mouse IgG (Santa Cruz Biotechnology). The signal was detected by the Western Lightning Plus-ECL kit (PerkinElmer, Wellesley, MA). Each experiment was repeated two times according to our previous method (22).

Statistics. Normally distributed data are expressed as means \pm SE and assessed for significance by Student's *t*-test or ANOVA as indicated with Bonferroni correction for multiple comparisons.

RESULTS

Decellularized rat lung slices retain anatomical integrity. Our prior studies indicated that organotypic tissue-engineered lungs could be constructed in biomimetic bioreactor and that acellular rat lung scaffolds contain the appropriate three-dimensional (3D) architecture and regional-specific cues for cellular adhesion and growth (23). Given the central role of fibroblasts in the regulation of lung homeostasis and ECM dynamics, we wished to adapt this system for the *in vitro* study of fibroblast biology. We chose to first start with the rat system because, to date, rat lung is the only mammalian scaffold system that has been used successfully for implantable, functional, bioartificial lung. However, because the quantities of input cells required to study cultured or primary fibroblast in the bioreactor would be prohibitive and difficult to adapt for widespread use, we pursued a method to culture cells in smaller pieces of scaffold, namely, slices. Rat lung was decellularized according to our previously published methods and sliced into 2-mm slices suitable for tissue culture (Fig. 1, A and B). As shown in Fig. 1, C and D, hematoxylin and eosin (H&E) staining and scanning electron microscopy (SEM) analysis confirmed that scaffold slices demonstrate intact alveolar architecture and the complete absence of cells. These data show that decellularized rat lungs can be processed into smaller slices potentially suitable for cell culture.

Development of an objective cell growth scoring standard. Having found that rat lung scaffolds retained their architecture

following slicing in this manner, we next sought to determine whether these scaffolds could support fibroblast growth. Here, 1×10^4 , 1×10^5 , and 1×10^6 cells from the mouse fibroblast A9 cell line were inoculated in medium onto the slice (Fig. 1E) and allowed to grow for between 1 to 14 days. At serial time points, scaffolds were harvested, fixed, and assessed for evidence of fibroblast engraftment. In our pilot work, examination of the seeded scaffolds revealed that the presence of cells was not uniform throughout the section. To overcome this limitation and provide a more representative and standardized method of reporting cellular content in this system, we developed a semiquantitative scoring system that would account for uneven cell distribution in two dimensions. We called this objective scoring standard the repopulation index. Here, percentages of scaffold-containing cells were manually determined for the entire cultured slice, and scores between 0 and 5 were assigned based on the cell density detected in the scaffold. The scoring approach was used because, under certain conditions, some regions of the scaffold displayed such a high cell content and density that determination of precise cell counts was not possible. Additionally, the nonuniform engraftment required a method that would take into account all regions of the tissue. Images at $\times 10$ were captured, and the following system was employed. When between 10–20% of tissue contained cells, the score was 1. When 20–30% was covered, the score was 2. When 30–40% was covered, the score was 3. When 40–50% was covered, the score was 4. When the score exceeded 50%, the score was 5. For regions containing <1% of coverage, a score of 0.1 was assigned when 3 to 6 cells were observed in measured tissue area, a score of 0.25 was assigned when 10 to 15 cells were counted in measured area, a score of 0.5 was assigned when 20 to 25 cells in measured tissue area were seen, and a score of 0.75 was conferred when 35 to 40 cells were detected in the measured tissue area. We made this adjustment to avoid the overstatement of results that might occur should a score of 1 be conferred upon any percentage of tissue density between 0.1% to 10%. Next, because each image did not capture the entire tissue slice, scores were multiplied by the percent area in which they were measured and finally added to derive the final score. At least three separate slices were scored for each animal, and these final scores were then averaged to obtain a mean for each group studied. Low-power representative images for some of these scores are shown in Fig. 2C. These data indicate that development of an objective scoring standard may be used in studies of lung bioengineering. Although this index may not be applicable in all studies, it represents a potential advance in terms of methods of quantification of cell engraftment.

This approach found that, at the 24-h time point, repopulation in the 10^6 seeded sample was significantly increased above both the 10^4 seeded sample ($P < 0.01$) and the 10^5 seeded sample ($P < 0.05$) but that no difference was detected between the 10^4 and 10^5 values. At the 72-h time point, the 10^5 sample no longer exceeds the 10^4 sample, but the 10^6 value still exceeds the 10^4 value ($P < 0.05$). At the 5-day time point, engraftment in the 10^4 seeded scaffold approximates the 10^5 and 10^6 samples and is increased from the baseline 10^4 value ($P < 0.05$). From 7 days onward, the 10^4 , 10^5 , and 10^6 samples are equivalent and the 10^4 sample continues to be increased from 24 h ($P < 0.05$). At days 10 and 14, the 10^5 and 10^6 samples reach significant increase from the corre-

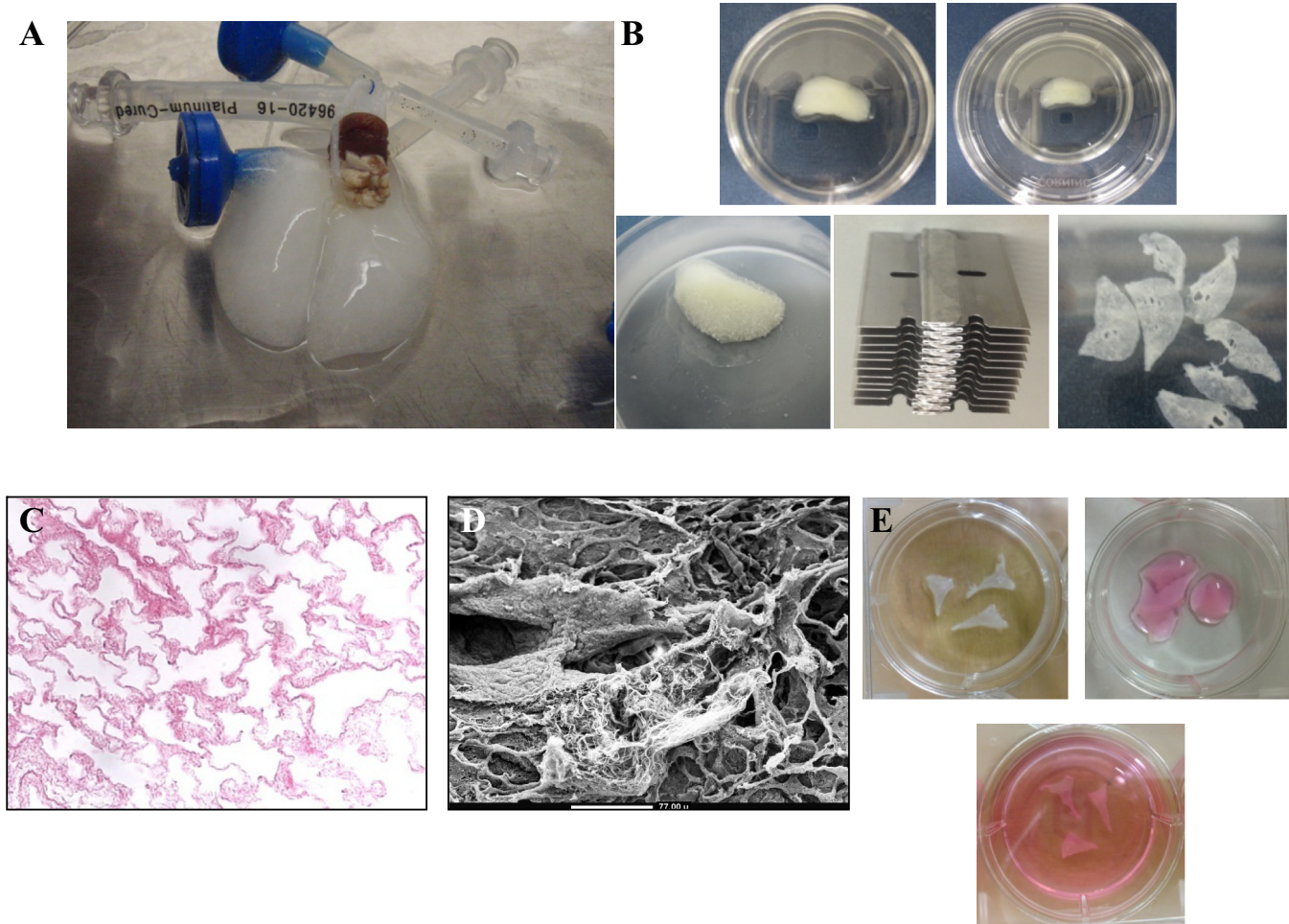


Fig. 1. *A*: gross appearance of decellularized rat lung. *B*: slicing procedure. Clockwise from top left: 1) intact lung scaffold is placed in 60-mm Petri dish; 2) scaffold containing dish is placed in a 100-mM Petri dish and floated in liquid nitrogen; 3) scaffold is now frozen and hard enough to slice consistently; 4) cutting tool fashioned from razor blades used for consistently sized slices; 5) resulting scaffold slices. *C*: hematoxylin and eosin (H&E). *D*: scanning electron microscopy (SEM) of the scaffold slices reveals intact alveolar architecture. *E*: procedure for inoculating rat lung scaffold slices with fibroblasts. Clockwise from top left: 1) slices are placed in poly-L-lysine-coated 6-well plate, extended with forceps, incubated at 37°C × 10 min, and then 2) inoculated with 100 μ l of cell-containing medium. Plates were incubated at 37°C × 30 min. 3) 1.7 additional ml of medium was added to the well, and plates were placed into incubator.

sponding baseline values ($P < 0.05$). Due to statistical corrections for multiple comparisons, no other comparisons reached significance. Graphical representation of these data is shown in Fig. 3A.

Decellularized rat lung slices support survival, proliferation, and collagen production of seeded fibroblasts. Based on these data, it seemed that 10^5 cells appeared to be the optimum dose for cell seeding in terms of two-dimensional initial engraftment. Thus further functional assessment of seeded cells was performed at this dosage. The finding that fibroblast quantities increased over time suggested that fibroblasts could both survive and proliferate in decellularized rat lung slices. To ascertain whether this assumption was valid, we assessed fibroblast cell death by TUNEL staining and fibroblast proliferation by Ki67 immunostaining at serial time points during seeding and culture. Here we found little to no detectable TUNEL signal after 24 h of culture and only very few cells exhibiting TUNEL signal after 7 and 14 days (Fig. 4A). In contrast, strong and persistent Ki67 staining was detected in nearly all cells at all time points following cell seeding (Fig. 4, A and B) in all groups although the intensity of staining of

individual cells was unchanged between the 10^4 , 10^5 , and 10^6 seeded scaffolds at all time points (Fig. 4B). Taken together, these data indicate that, following the initial adhesion and engraftment, A9 cells grow robustly in the rat lung scaffold.

In considering these data, we noticed that two-dimensional detection of cells appeared to level off over time but that nearly all cells expressed Ki67 (indicating that nearly all cells were proliferative), and nearly no cells exhibited TUNEL signal (meaning that nearly all cells were viable). This observation might be explained by downward growth of the cells into the scaffold. To determine whether this assumption was correct, experiments were repeated, and scaffolds were sectioned sagittally. Microscopic examination of these sections revealed the appearance of cells in the lower parts of the scaffold at later time points (Fig. 4C and data not shown), indicating that, in addition to engraftment in a two-dimensional fashion, cells seeded in this manner can migrate down into the matrix.

One critical function of fibroblasts is the synthesis and deposition of ECM proteins that maintain lung architecture and stability. To determine whether A9 fibroblasts displayed this function in the decellularized rat lung slices, collagen produc-

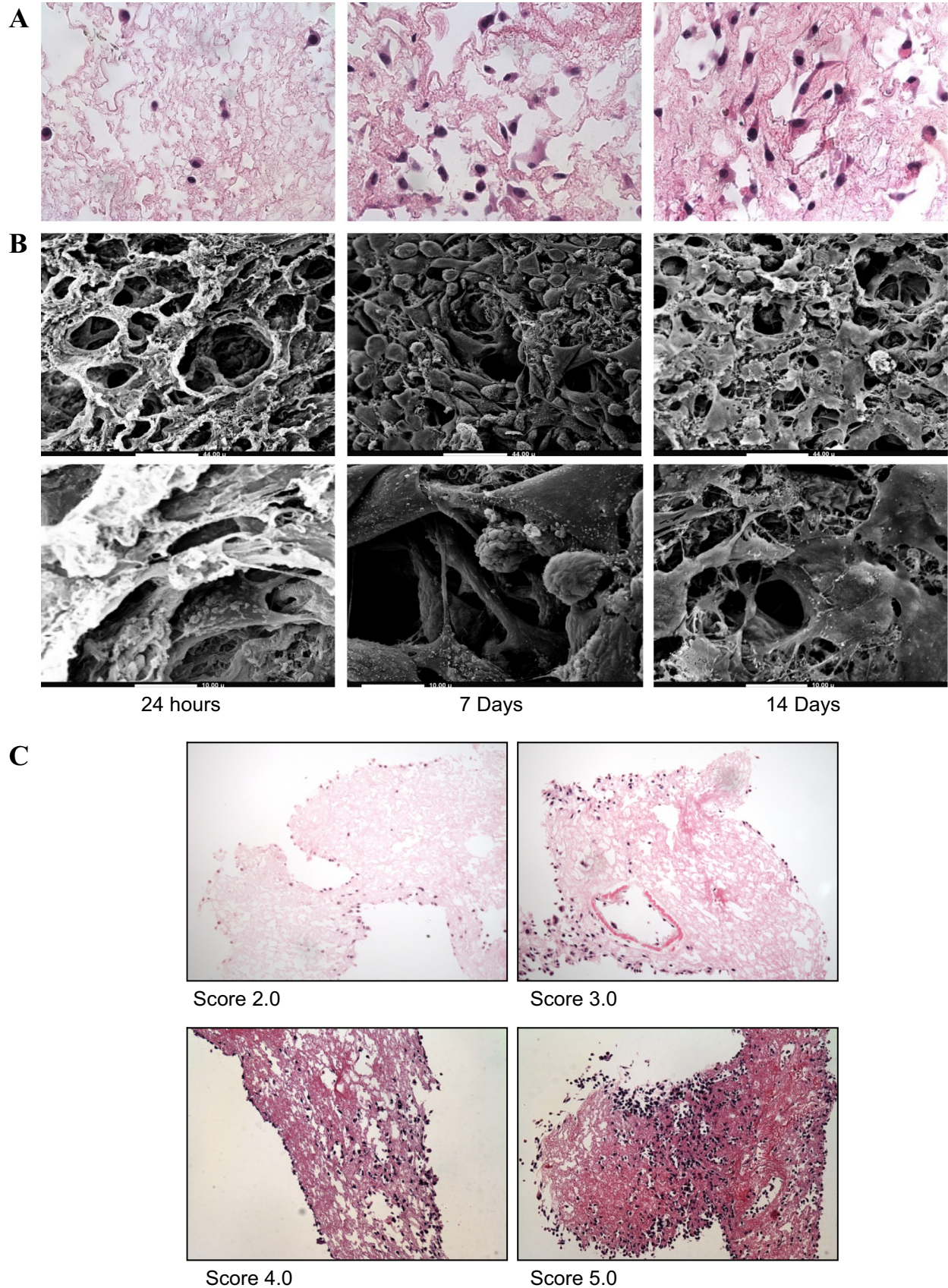


Fig. 2. *A*: H&E staining. *B*: SEM of rat scaffold slices seeded with mouse A9 fibroblasts demonstrates a time-dependent increase in cells. H&E images are $\times 40$ original magnification. In the low-power, lower-SEM images, the bar represents $44\ \mu\text{m}$ and in the high-power view scale bar represents $10\ \mu\text{m}$. *C*: representative H&E images of the repopulation index developed for standardized reporting of cellular engraftment in this model. Images are $\times 10$ original magnification.

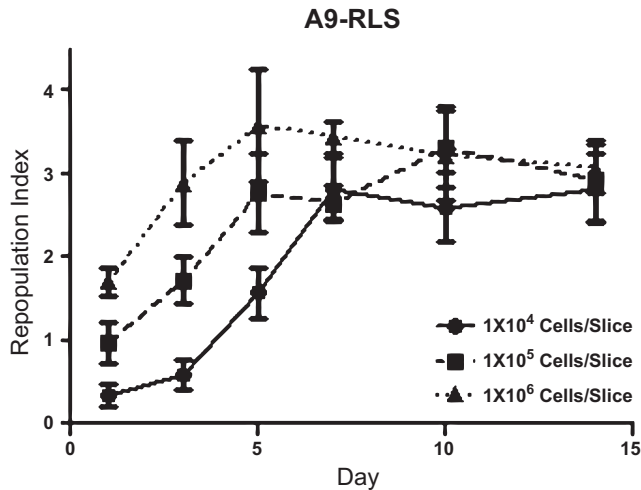


Fig. 3. Comparison of repopulation index at early and late time points in the setting of different amounts of seeded cells. ●: 1×10^4 cells/slice. ■: 1×10^5 cells/slice. ▲: 1×10^6 cells/slice. At the 24-h time point, the 10^6 repopulation is significantly increased above the 10^4 seeded sample ($P < 0.01$) and the 10^5 seeded sample ($P < 0.05$). No difference is seen in the 10^4 and 10^5 values. At the 72-h time point, the 10^5 sample no longer exceeds the 10^4 sample, but the 10^6 value still exceeds the 10^4 value ($P < 0.05$). At the 5-day time point, the 10^4 seeded scaffold is increased from baseline ($P < 0.05$) and now approaches the 10^5 and 10^6 samples. From day 7 on, the 10^4 , 10^5 , and 10^6 samples are equivalent, and the 10^4 sample continues to be increased from 24 h ($P < 0.05$). At days 10 and 14, the 10^5 and 10^6 samples reach significant increase from the corresponding baseline values ($P < 0.05$). Due to statistical corrections for multiple comparisons, no other comparisons are significant.

tion and deposition were evaluated using immunofluorescence detection of procollagen I α 1 and Masson Trichrome staining. As shown in Fig. 4, A and D, persistent procollagen I α 1 staining was detected at all time points in all groups studied following cell seeding. This finding was accompanied by the accumulation of collagen and detected by Masson trichrome staining in the later time points studied (Fig. 4E). In fact, in many regions of the lung in the later samples, changes reflecting excessive ECM could be detected (Figs. 2C and 4E). These data indicate that dermal fibroblasts do engraft in decellularized rat lung scaffolds, where they produce ECM components such as collagen, but that this engraftment is accompanied by architectural disruption and ECM accumulation commonly seen in fibrotic lung disease.

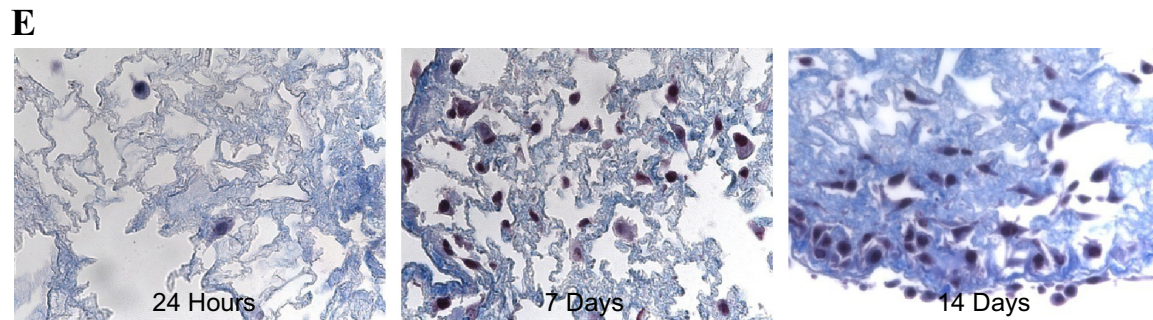
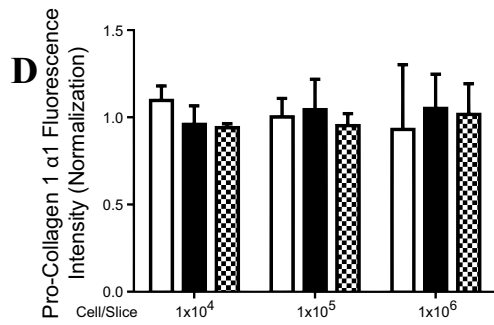
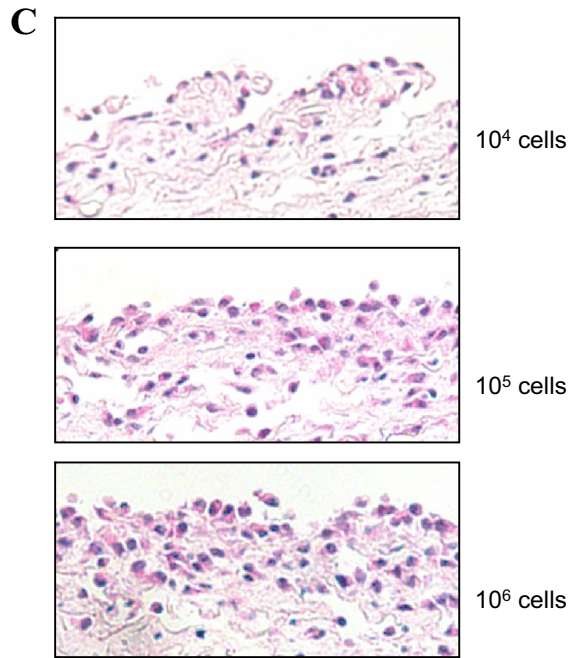
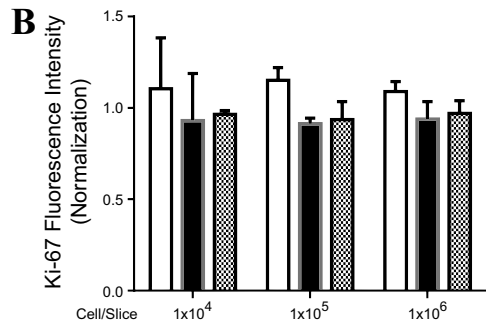
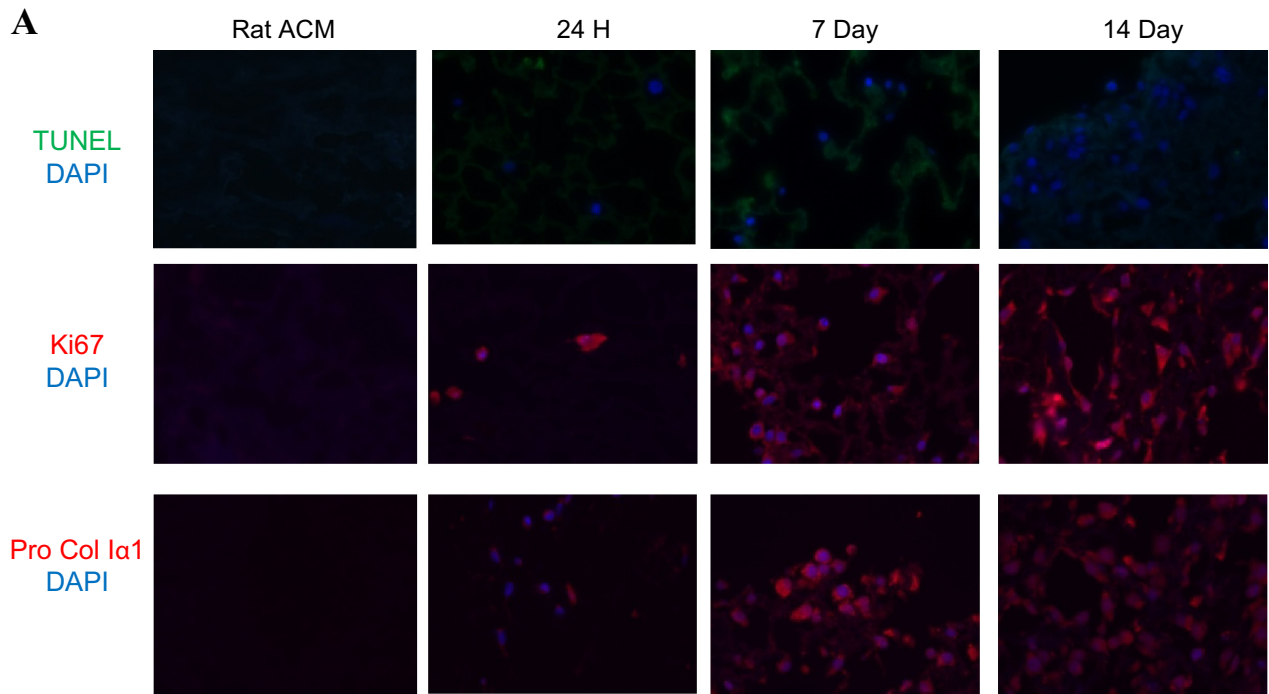
Decellularized mouse lung slices retain anatomic and biochemical integrity. These data indicate that decellularized rat lung scaffold slices support the growth and function of cultured A9 mouse fibroblasts. However, because we were concerned about a potential xenograft mismatch effect of growing mouse cells in rat lungs, we wished to further adapt this technique for the study of lung biology for which mouse modeling is currently widespread. We also wished to streamline the process of lung decellularization to enable dissemination of this method,

and, perhaps most importantly, we wished to establish a method of processing that did not require an intact lung that could be used for mechanistic studies in the setting of the limited starting material likely to be encountered in the setting of human lung engineering. For all of these reasons, we sought to simplify the lung decellularization process. To achieve this goal, we started by harvesting lung tissue from adult C57BL/6 mice. As shown in Fig. 5A, following right ventricular perfusion, intact lungs were removed en bloc, and lobes were snap frozen and cut into 2-mm slices. Slices were placed in decellularization solution, and DNA was digested by benzonase. Slices were then extensively rinsed with PBS containing 2% gentamycin and 10% penicillin/streptomycin.

Analysis of the resulting mouse lung scaffold slices by H&E and DAPI staining revealed that the cells and nuclear material were removed with the decellularization process, but the alveolar septal architecture persisted (Fig. 5B). SEM demonstrated that parenchymal and blood-borne cells seen in native lung were absent in the decellularized scaffold (Fig. 5B). DAPI staining and fluorometric DNA quantification indicated that ~98% of DNA was removed by the decellularization process (Fig. 5, C and D), and immunoblotting for MHC-II as well as β -actin confirmed that decellularized mouse lung scaffolds were depleted of these cellular markers (Fig. 5E). Immunofluorescence and immunohistochemical staining indicated that collagen, elastin, laminin, and fibronectin were preserved in decellularized matrices, but most sulfated GAGs were removed (Fig. 6). These data indicate that decellularization of mouse lung slices produces an acellular matrix, which retains most of the gross and microstructural properties of native lung, yet removal of cellular components is complete.

Decellularized mouse lung slices support mouse lung fibroblast growth. We next determined whether scaffolds prepared in this manner could support fibroblast cell growth. Here, 1×10^4 , 1×10^5 and 1×10^6 A9 cells were seeded in medium on the slice (Fig. 7A) and allowed to grow for 1 to 14 days. Slices were harvested at sequential time points and assessed for cell content by H&E staining and SEM. As with the rat matrix described above, here we found that A9 cells could also survive and expand in the mouse lung scaffold in a time-dependent manner (Fig. 7, B–D). For example, the 24-h time point demonstrates that the 10^4 seeded sample shows significantly less repopulation than those seeded with 10^5 ($P < 0.05$) or 10^6 ($P < 0.01$) cells, and there is no difference in the index between the scaffolds seeded with 10^5 or 10^6 cells. At the 72-h data point, the 10^4 seeded sample again displays a lower index than the corresponding 10^5 and 10^6 seeded scaffolds ($P < 0.01$ both comparisons), which are both increased from 24 h ($P < 0.05$). At the 5-day, 7 day, 10-day, and 14-day time points, the 10^4 , 10^5 , and 10^6 seeded scaffolds demonstrate equivalent engraftment. The 10^4 sample displays higher repopulation scores than the corresponding 24- and 72-h time points ($P <$

Fig. 4. A: immunofluorescence staining for TUNEL (green, top), Ki67 (red, middle), and procollagen I α 1 (red, bottom) indicates minimal cell death at all time points, but robust Ki67 and Pro-Col I α 1 detection in rat lung scaffold slices were seeded with A9 mouse fibroblasts. ACM: acellular matrix. B: quantification of mean fluorescence intensity of Ki67 immunostaining reveals similar signal in all groups at all time points. C: representative images of scaffolds seeded with 10^4 , 10^5 , or 10^6 cells, incubated for 14 days, and analyzed for depth of migration by seeded A9 cells. For each time point, at least 3 slices were evaluated. $\times 10$ original magnification. D: quantification of mean fluorescence intensity of Pro-Col I α 1 staining reveals similar signal in all groups at all time points. E: trichrome staining at early and late time points demonstrates accumulation of collagen. With the exception of C, all images are $\times 40$ original magnification, and at least 3 slices were assessed.



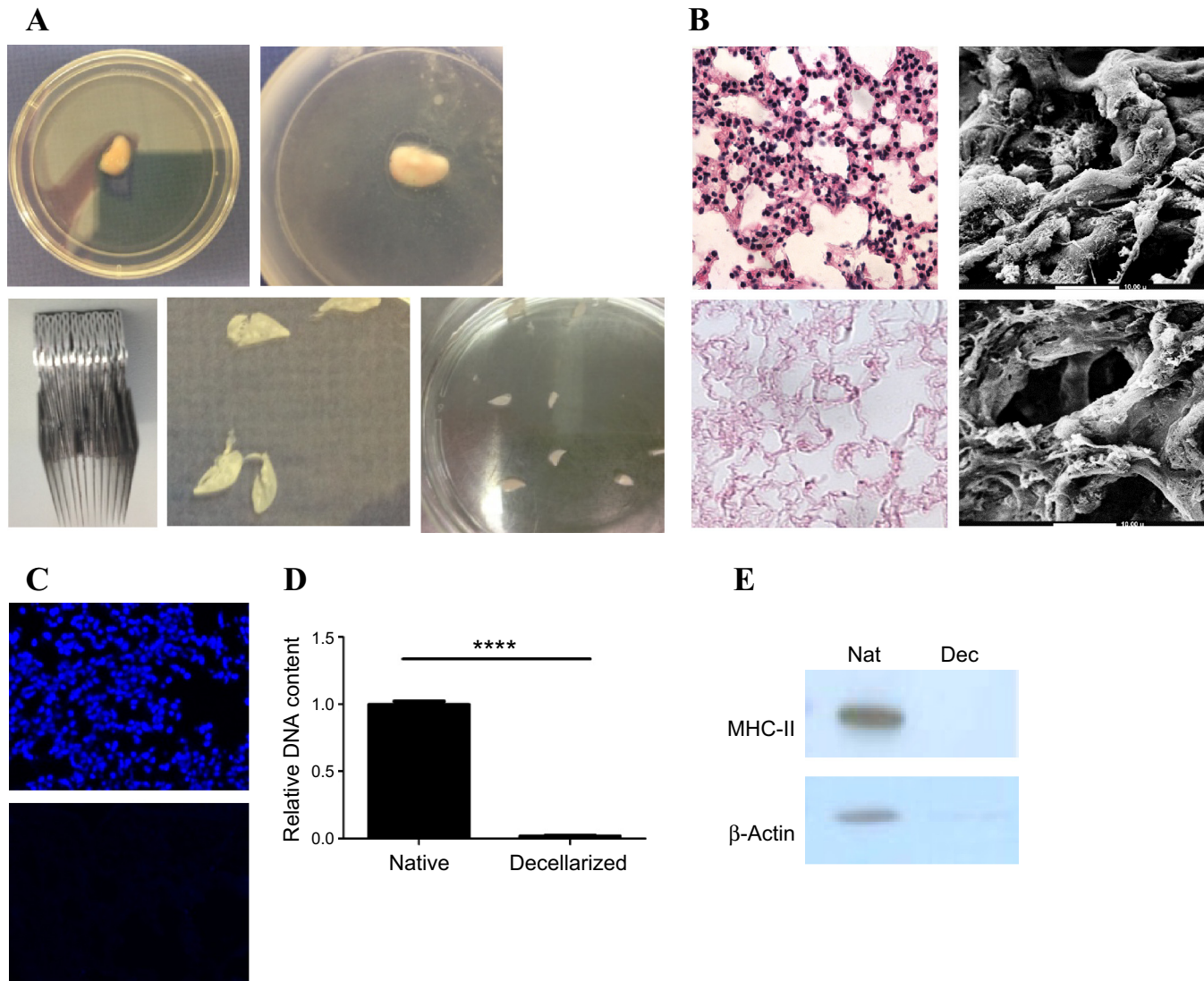


Fig. 5. *A*: preparation of decellularized mouse lung slices. Clockwise from top left: 1) lavaged and perfused mouse lung is placed in a 60 mm Petri dish; 2) lung containing dish is placed in a 100-mm petri dish and floated on liquid nitrogen to snap freeze the lung; 3) frozen lung is cut into slices by multiknife; 5) larger view of slices, multiknife apparatus fashioned out of razor blades for accurate simultaneous cutting. *B*: H&E staining (*left*) and SEM (*right*) of native lung (*top*) and decellularized lung (*bottom*) indicates that the appearance of cellular components is absent from the decellularized lung slice. *C* and *D*: DNA content analysis by DAPI (*C*) nuclear counterstaining and fluorometric quantification (*D*) of digested scaffold indicates that DNA is absent from the decellularized matrix (**** $P < 0.0005$). *E*: Western blot analysis for major histocompatibility complex II (MHC-II) and β -actin reveals that immunogenic and cellular proteins are absent from the decellularized lung.

0.05), but the 10^5 and 10^6 values are not increased above that noted at any previous time point. No other comparisons are found to be significant, and at all time points the 10^5 and 10^6 seeded samples exhibited nearly identical two-dimensional engraftment (Fig. 7D). Furthermore, as with the reseeded rat lung, ECM accumulation and fibrosis-like changes were also seen at the later time points (Fig. 7B).

Initial fibroblast:matrix interactions in decellularized mouse lung slices are $\beta 1$ -integrin, FAK, and ERK dependent and are opposed by AKT. Having fully established this culture system, we last turned our attention to investigating the molecular mechanism(s) governing fibroblast interactions with the mouse lung scaffold. As shown above, the decellularization process preserves collagen, fibronectin, and laminin, which led us to reason that a major ligand of these proteins, the $\beta 1$ -integrin

subunit, was at least partially involved in cellular engraftment. To test this hypothesis, we used a well-validated blocking antibody to inhibit $\beta 1$ -integrin binding and activation in this system. Here, as expected, after 24-h treatment, we found a 61.5% reduction in the repopulation index in the mouse lung scaffolds treated with $\beta 1$ -integrin-blocking antibody compared with those treated with isotype control ($P = 0.03$, Fig. 8A). Because initial adherence and survival would be expected to influence longer-term outcomes, we chose to restrict our analysis to the initial events following cell seeding. These data indicate that the initial engraftment of fibroblasts in this model occurs in a $\beta 1$ -integrin-dependent fashion.

Integrin signaling pathways are complex and significantly influenced by crosstalk with growth factor receptors. One of the signaling molecules involved in integrin-mediated cell

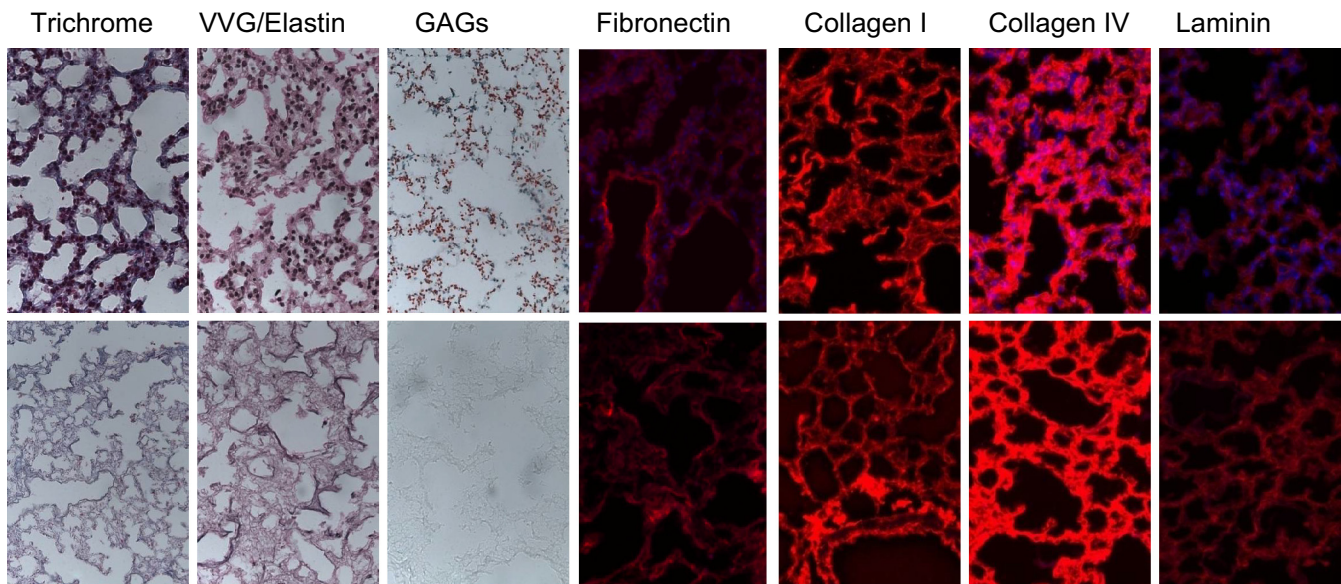


Fig. 6. Comparison of extracellular matrix proteins in native (*top*) vs. decellularized (*bottom*) mouse lung slices. All images are $\times 40$ original magnification. Fluorescence images are counterstained with DAPI. VVG, Verhoeff Van Gieson; GAG, glycosaminoglycan.

survival is FAK, which is activated following integrin ligation. Because FAK is required for cytoskeleton stabilization and is known to importantly regulate fibroblast adhesion and survival in other systems, we thought it likely that FAK might be involved in our system as well. This prediction proved correct, as, when A9 cells were seeded into the acellular scaffold slices and grown in the presence of FAK inhibitor 14, the appearance of cells was reduced in a dose-dependent fashion, such that, in the presence of $10 \mu\text{M}$ FAK inhibitor, repopulation scores were reduced by 72.3% ($P = 0.002$, Fig. 8B).

FAK is known to regulate fibroblast adhesion in a manner that involves activation of several downstream kinases, including ROCK, ERK, and the phosphatidylinositol 3-kinase/AKT signaling cascade. We thought it possible that some or all of these pathways were involved in our observed effects. To test this hypothesis, the 24-h culture experiments were repeated in the presence of escalating concentrations of specific inhibitors of ROCK, ERK, and AKT. Here we found that ROCK inhibition had no effect at any dose tested (Fig. 8C), that ERK inhibition reduced the repopulation index at 24 h by more than 2.4-fold ($P = 0.04$, Fig. 8D), and that low-dose AKT inhibition actually increased repopulation scores by more than 2.4-fold ($P = 0.01$, Fig. 8E). This effect was not observed at higher concentrations tested. This unexpected effect appeared to be related to increased ERK phosphorylation, as the immunofluorescence detection of pERK was stronger in the scaffolds treated with $25 \mu\text{M}$ AKT inhibitor compared with samples treated with either no inhibitor or with higher concentrations (Fig. 8F).

DISCUSSION

These data lend new insight into the mechanisms controlling fibroblast adhesion and survival in the decellularized rodent lung. Specifically, they indicate that decellularized rat lung scaffold slices can support the growth and survival of a mouse fibroblast cell line, that decellularized mouse lung slices demonstrate similar biochemical and growth-supporting properties,

but that these functions are accompanied by collagen accumulation and the histological appearance of fibrosis. Initial engraftment of fibroblasts in the decellularized mouse lung occurs via a $\beta 1$ -integrin-, FAK-dependent pathway that is mediated by ERK and opposed by AKT. Taken together, these data provide important information regarding the kinetics and mechanism through which seeded fibroblasts repopulate the decellularized rodent lung and are highly relevant for studies of tissue regeneration and ex vivo bioengineered lung, which relies on an intact and functional ECM.

Acellular rodent lungs were initially developed as a platform to support the in vitro regeneration of functional lung tissue (19, 23). In these initial studies, intact rat lung was decellularized through the vascular bed and transferred to a bioreactor, where it was seeded with epithelial and endothelial cells. One major factor limiting graft function in this system is vascular leak, which could be ameliorated by the administration of mesenchymal cells, such as fibroblasts, which would be expected to support the repair and regeneration of injured areas (29). Fibroblasts would also be expected to influence the engraftment and survival of epithelial populations through the production of ECM, by direct cellular interactions, as well as through paracrine effects (13). Thus study of fibroblast:matrix interactions have the potential to advance the development of bioengineered lungs. Our results are not directly applicable to studies of decellularized whole lung grown in the bioreactor, but they do provide a starting point for evaluating the mechanism through which instilled fibroblasts adhere and initially survive in this model.

The lung slice method reported herein has many potential uses in mechanistic studies of adhesion, survival, motility, and proliferation of a variety of cell lineages. First, the technology is not as labor intensive or costly as bioreactor studies and therefore can be adapted for use in many types of laboratories. The method can be used in the setting of very small amounts of starting material unlike the bioreactor approach, which requires large numbers of infused cells. The method is also

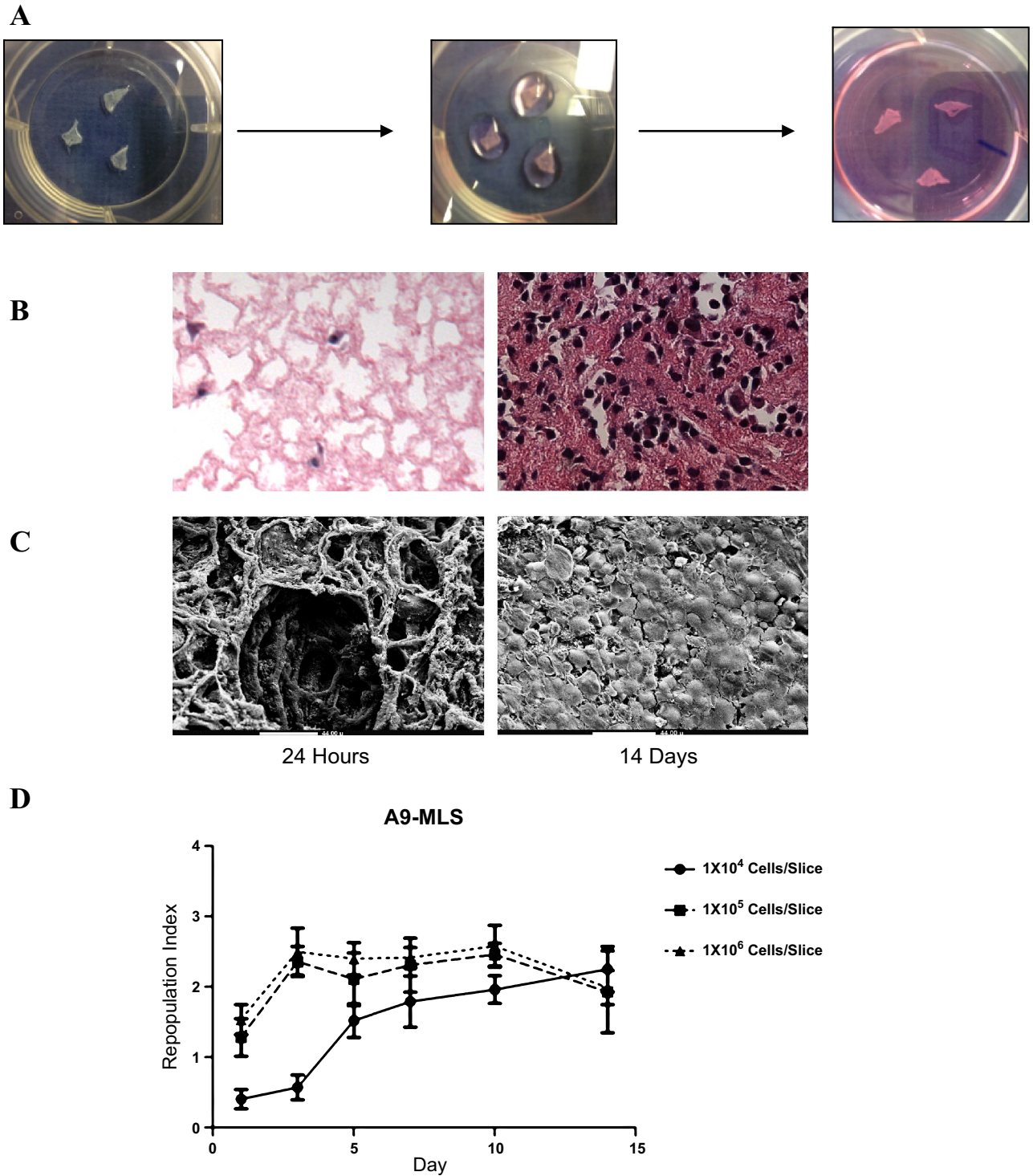


Fig. 7. *A*: procedure for seeding decellularized mouse lung slices with cells. Cells are placed in poly-L-lysine-coated 6-well plate, extended with forceps, incubated at 37°C × 10 min and then inoculated with 50 μl of cell-containing medium. Plates were incubated at 37°C for 30 min. 1.85 additional ml of medium was added to the well, and plates were placed into incubator. *B*: H&E staining demonstrates a differences in fibroblasts cultured in this manner at early vs. late time points. *C*: SEM reveals a similar time-dependent increase in seeded fibroblasts. *D*: quantification of repopulation index throughout the course of the study. At the 24-h data point, the 10⁴ seeded sample shows significantly less repopulation than those seeded with 10⁵ ($P < 0.05$) or 10⁶ ($P < 0.01$) cells. At this time point, there is no difference in the index between the scaffolds seeded with 10⁵ or 10⁶ cells. At the 72-h data point, the 10⁴ seeded sample again displays a lower index than the corresponding 10⁵ and 10⁶ seeded scaffolds ($P < 0.01$ both comparisons), which are both increased from 24 h ($P < 0.05$). At the 5-day, 7-day, 10-day, and 14-day time points, the 10⁴, 10⁵, and 10⁶ seeded scaffolds demonstrate equivalent engraftment. The 10⁴ sample displays higher repopulation scores than the corresponding 24- and 72-h time points ($P < 0.05$), but the 10⁵ and 10⁶ values are not increased above that noted at any previous time point. Due to statistical corrections for multiple comparisons, no other comparisons are significant. Additionally, at all time points, the 10⁵ and 10⁶ seeded samples exhibited nearly identical 2-dimensional engraftment. H&E images are ×40 original magnification. In the SEM images, the bar represents 10 μm.

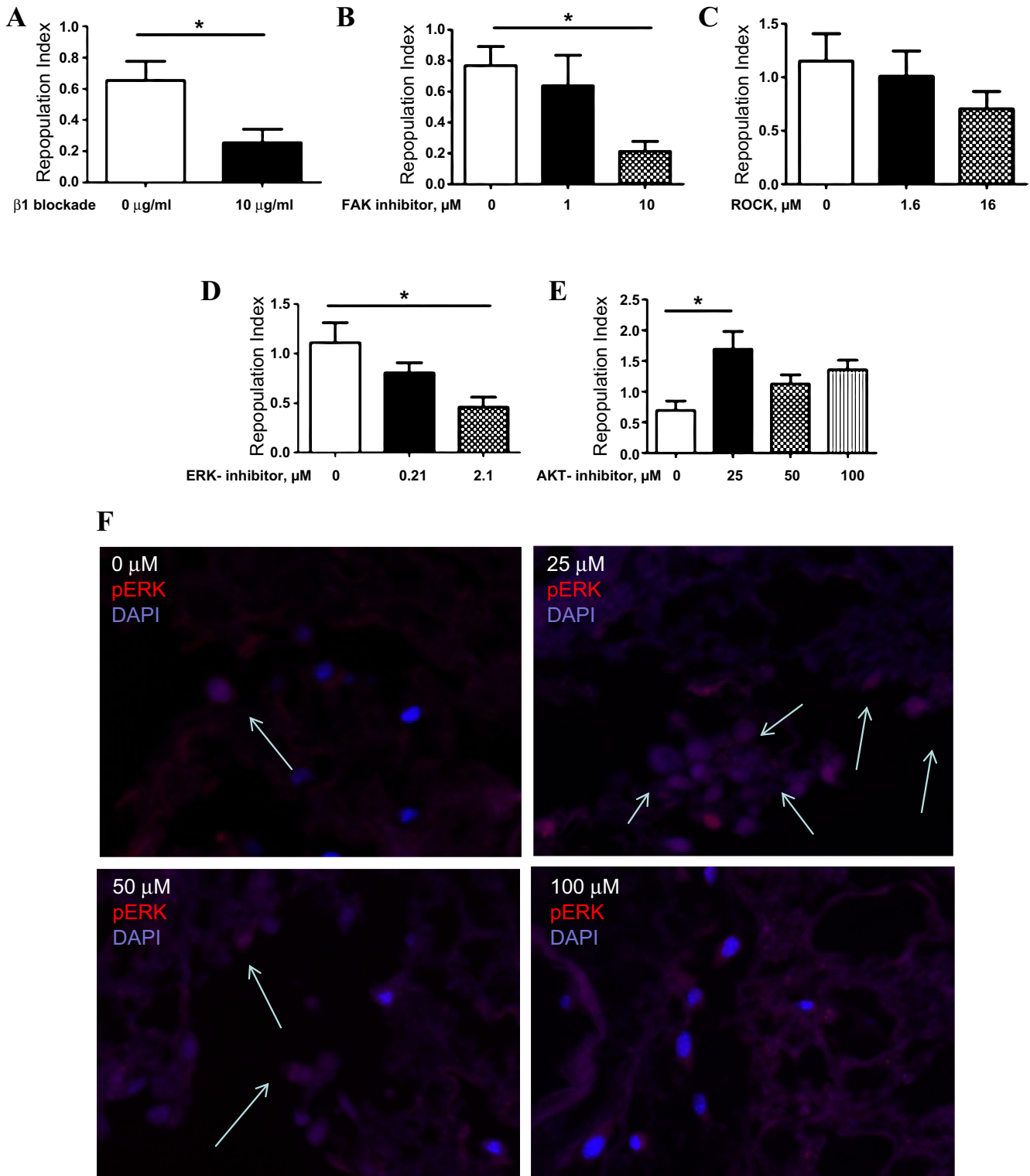


Fig. 8. Treatment of fibroblast seeded mouse lung slices with β 1-integrin-blocking antibody leads to a significant reduction in the mean repopulation index (A). B: treatment of fibroblast seeded decellularized mouse lung slices with 10 μ M focal adhesion kinase (FAK) inhibitor significantly reduces repopulation scores. C: treatment of fibroblast seeded mouse lung slices with Rho-associated kinase (ROCK) inhibitor does not affect the repopulation index. D: treatment of fibroblast seeded decellularized mouse lung slices with 2.1 μ M ERK inhibitor significantly reduces repopulation scores. H&E images are $\times 10$ original magnification. E: treatment of fibroblast seeded mouse lung slices with AKT inhibitor reveals an increase in the repopulation index in the cells treated with low concentrations (25 μ M) of AKT inhibition. F: immunofluorescence of seeded scaffolds treated with AKT inhibitor at a doses of 0 μ M, 25 μ M, 50 μ M, and 100 μ M. Red: pERK. Blue: DAPI. The arrows indicate pERK containing nuclei. * $P < 0.05$.

suitable for coculture studies, which will allow study of both cell:cell and paracrine interactions between the various cell populations comprising the lung and is also amenable for high-throughput screening. Last, this method also holds great potential for use in mechanistic evaluation using fresh tissue obtained from living or deceased humans, where starting material is scarce.

In these studies, we find that initial adhesion is mediated by β 1-integrin and FAK via an ERK-dependent pathway. Curiously, low-dose AKT inhibition increases ERK phosphorylation and increases the initial repopulation score, which is consistent with findings in other cell culture systems in which AKT activation impedes ERK phosphorylation (5). Furthermore, although AKT is generally thought of as downstream of FAK in the setting of β 1-integrin activation (35), one recent report indicates that, in some settings, AKT might stimulate FAK activation (32). Because both ERK and AKT are known to regulate fibroblast proliferation in the setting of profibrotic stimuli (17, 36), it is likely that inhibition of AKT at later time points would attenuate fibroblast survival and expansion or that addition of certain growth factors to the culture medium would lead to different results. Further work will be required to confirm this hypothesis and to better understand the relationship of β 1-integrin, FAK, and its downstream signaling pathways in our modeling system, as well the contribution of other integrin subunits, heterodimers, and signaling pathways. In addition, given the apparent fibrosis that developed at later time points in these studies, the factors controlling proliferation and collagen require significant study in order that this method might be useful in the construction of functional lung tissue.

One very interesting aspect of our study was that the A9 fibroblasts demonstrated robust growth that increased because, as time progressed, both the rat and mouse lung scaffolds resembled fibrotic lung with the accumulation of collagen and highly proliferative fibroblasts. The unopposed cell growth and collagen accumulation seen in our model likely relate to our use of an immortalized cell line although it is also possible that the lack of other resident lung cell populations and presumably a disrupted basement membrane contributed to these effects. Because the ultimate goal of this work is the generation of normal lung tissue that will support gas exchange, this finding underscores the need to harness these aspects of fibroblast function so that their repopulation in the decellularized lung occurs in a controlled and beneficial manner. This issue could be further interrogated using genetically modified fibroblasts or gene knockdown strategies combined with studies of receptor-ligand interactions. Similarly, future work using primary lung fibroblasts, as well as coculture experiments involving fibroblasts and epithelial cells, will help elucidate this matter.

Despite these advances, several caveats exist. We have not determined whether this method is suitable for the study of fibrotic or emphysematous mouse lung, in which matrix abnormalities may impede the decellularization procedure or lead to loss of ECM components. This method also will not allow study of the lung as an intact unit or the study of biomechanics including inflation, deflation, mechanical stretch, and blood flow. We have also not determined the α -subunit and other β -integrin isoforms that might be important in our system. Last, we have also not examined the interaction of fibroblasts with the structural and inflammatory cells that would be expected to participate in bidirectional crosstalk and mediate

repair. Nevertheless, despite these limitations, our approach provides significant insight into the factors controlling initial fibroblast:matrix interactions in the decellularized mouse lung and serve as an important starting point for future studies in this area.

GRANTS

This work was supported by NIH HL109033 and the Translational Lung Research Program at Yale School of Medicine (both E. Herzog) and R01HL098220-01 and 1U01HL111016-01 (both L. Niklason).

DISCLOSURES

No conflicts of interest, financial or otherwise, are declared by the authors.

AUTHOR CONTRIBUTIONS

Author contributions: H.S. and E.L.H. conception and design of research; H.S., E.A.C., X.C., A.M., Y.Z., J.M., L.Z., X.P., and H.P. performed experiments; H.S., E.A.C., X.C., A.M., Y.Z., J.M., X.P., H.P., and E.L.H. analyzed data; H.S., A.M., L.E.N., X.P., H.P., and E.L.H. interpreted results of experiments; H.S. and E.L.H. prepared figures; H.S. and E.L.H. drafted manuscript; H.S., E.A.C., A.M., and E.L.H. edited and revised manuscript; H.S., E.A.C., X.C., A.M., Y.Z., J.M., L.Z., L.E.N., X.P., H.P., and E.L.H. approved final version of manuscript.

REFERENCES

1. Bonenfant NR, Sokocevic D, Wagner DE, Borg ZD, Lathrop MJ, Lam YW, Deng B, Desarno MJ, Ashikaga T, Loi R, Weiss DJ. The effects of storage and sterilization on de-cellularized and re-cellularized whole lung. *Biomaterials* 34: 3231–3245, 2013.
2. Booth AJ, Hadley R, Cornett AM, Dreffs AA, Matthes SA, Tsui JL, Weiss K, Horowitz JC, Fiore VF, Barker TH, Moore BB, Martinez FJ, Niklason LE, White ES. Acellular normal and fibrotic human lung matrices as a culture system for in vitro investigation. *Am J Respir Crit Care Med* 186: 866–876, 2012.
3. Bowden DH, Young L, Adamson IY. Fibroblast inhibition does not promote normal lung repair after hyperoxia. *Exp Lung Res* 20: 251–262, 1994.
4. Calle EA, Petersen TH, Niklason LE. Procedure for lung engineering. *J Vis Exp* 8: 2651, 2011.
5. Dai R, Chen R, Li H. Cross-talk between PI3K/Akt and MEK/ERK pathways mediates endoplasmic reticulum stress-induced cell cycle progression and cell death in human hepatocellular carcinoma cells. *Int J Oncol* 34: 1749–1757, 2009.
6. Daly AB, Wallis JM, Borg ZD, Bonvillain RW, Deng B, Ballif BA, Jaworski DM, Allen GB, Weiss DJ. Initial binding and recellularization of decellularized mouse lung scaffolds with bone marrow-derived mesenchymal stromal cells. *Tissue Eng Part A* 18: 1–16, 2012.
7. De Filippo RE, Kornitzer BS, Yoo JJ, Atala A. Penile urethra replacement with autologous cell-seeded tubularized collagen matrices. *J Tissue Eng Regen Med*. In press.
8. Deng K, Gao Y, Cao Z, Graziani EL, Wood A, Doherty P, Walsh FS. Overcoming amino-Nogo-induced inhibition of cell spreading and neurite outgrowth by 12-O-tetradecanoylphorbol-13-acetate-type tumor promoters. *J Biol Chem* 285: 6425–6433, 2010.
9. Dunsmore SE, Rannels DE. Extracellular matrix biology in the lung. *Am J Physiol Lung Cell Mol Physiol* 270: L3–L27, 1996.
10. Gan Y, Reilkoff R, Peng X, Russell T, Chen Q, Mathai SK, Homer R, Gulati M, Siner J, Elias J, Bucala R, Herzog E. Role of semaphorin 7a signaling in transforming growth factor beta1-induced lung fibrosis and scleroderma-related interstitial lung disease. *Arthritis Rheum* 63: 2484–2494, 2011.
11. Golubovskaya VM, Nyberg C, Zheng M, Kweh F, Magis A, Ostrov D, Cance WG. A small molecule inhibitor, 1,2,4,5-benzenetetraamine tetrahydrochloride, targeting the y397 site of focal adhesion kinase decreases tumor growth. *J Med Chem* 51: 7405–7416, 2008.
12. Haykal S, Soleas JP, Salna M, Hofer SO, Waddell TK. Evaluation of the structural integrity and extracellular matrix components of tracheal allografts following cyclical decellularization techniques: comparison of three protocols. *Tissue Eng Part C Methods* 18: 614–623, 2012.
13. Herzog EL, Brody AR, Colby TV, Mason R, Williams MC. Knowns and unknowns of the alveolus. *Proc Am Thorac Soc* 5: 778–782, 2008.

14. Herzog EL, Van Arnam J, Hu B, Krause DS. Threshold of lung injury required for the appearance of marrow-derived lung epithelia. *Stem Cells* 24: 1986–1992, 2006.
15. Hynes RO. Integrins: bidirectional, allosteric signaling machines. *Cell* 110: 673–687, 2002.
16. Jungebluth P, Alici E, Baiguera S, Le Blanc K, Blomberg P, Bozoky B, Crowley C, Einarsson O, Grinnemo KH, Gudbjartsson T, Le Guyader S, Henriksson G, Hermanson O, Juto JE, Leidner B, Lilja T, Liska J, Luedde T, Lundin V, Moll G, Nilsson B, Roderburg C, Stromblad S, Sutlu T, Teixeira AI, Watz E, Seifalian A, Macchiarini P. Tracheobronchial transplantation with a stem-cell-seeded bioartificial nanocomposite: a proof-of-concept study. *Lancet* 378: 1997–2004, 2011.
17. Lu Y, Azad N, Wang L, Iyer AK, Castranova V, Jiang BH, Rojana-sakul Y. Phosphatidylinositol-3-kinase/akt regulates bleomycin-induced fibroblast proliferation and collagen production. *Am J Respir Cell Mol Biol* 42: 432–441, 2010.
18. Macchiarini P, Jungebluth P, Go T, Asnaghi MA, Rees LE, Cogan TA, Dodson A, Martorell J, Bellini S, Parnigotto PP, Dickinson SC, Hollander AP, Mantero S, Conconi MT, Birchall MA. Clinical transplantation of a tissue-engineered airway. *Lancet* 372: 2023–2030, 2008.
19. Ott HC, Clippinger B, Conrad C, Schuetz C, Pomerantseva I, Ikonomou L, Kotton D, Vacanti JP. Regeneration and orthotopic transplantation of a bioartificial lung. *Nat Med* 16: 927–933, 2010.
20. Patterson JT, Gilliland T, Maxfield MW, Church S, Naito Y, Shinoka T, Breuer CK. Tissue-engineered vascular grafts for use in the treatment of congenital heart disease: from the bench to the clinic and back again. *Regen Med* 7: 409–419, 2012.
21. Petersen TH, Calle EA, Colehour MB, Niklason LE. Bioreactor for the long-term culture of lung tissue. *Cell Transplant* 20: 1117–1126, 2011.
22. Petersen TH, Calle EA, Colehour MB, Niklason LE. Matrix composition and mechanics of decellularized lung scaffolds. *Cells Tissues Organs* 195: 222–231, 2012.
23. Petersen TH, Calle EA, Zhao L, Lee EJ, Gui L, Raredon MB, Gavrilov K, Yi T, Zhuang ZW, Breuer C, Herzog E, Niklason LE. Tissue-engineered lungs for in vivo implantation. *Science* 329: 538–541, 2010.
24. Regen CM, Horwitz AF. Dynamics of beta 1 integrin-mediated adhesive contacts in motile fibroblasts. *J Cell Biol* 119: 1347–1359, 1992.
25. Reilkoff RA, Bucala R, Herzog EL. Fibrocytes: emerging effector cells in chronic inflammation. *Nat Rev Immunol* 11: 427–435, 2011.
26. Reilkoff RA, Peng H, Murray LA, Peng X, Russell T, Montgomery R, Feghali-Bostwick C, Shaw A, Homer RJ, Gulati M, Mathur A, Elias JA, Herzog EL. Semaphorin 7a+ regulatory T cells are associated with progressive idiopathic pulmonary fibrosis and are implicated in transforming growth factor-beta1-induced pulmonary fibrosis. *Am J Respir Crit Care Med* 187: 180–188, 2013.
27. Sokocevic D, Bonenfant NR, Wagner DE, Borg ZD, Lathrop MJ, Lam YW, Deng B, Desarno MJ, Ashikaga T, Loi R, Hoffman AM, Weiss DJ. The effect of age and emphysematous and fibrotic injury on the re-cellularization of de-cellularized lungs. *Biomaterials* 34: 3256–3269, 2013.
28. Song JJ, Guyette JP, Gilpin SE, Gonzalez G, Vacanti JP, Ott HC. Regeneration and experimental orthotopic transplantation of a bioengineered kidney. *Nat Med* 19: 645–651, 2013.
29. Tager AM, LaCamera P, Shea BS, Campanella GS, Selman M, Zhao Z, Polosukhin V, Wain J, Karimi-Shah BA, Kim ND, Hart WK, Pardo A, Blackwell TS, Xu Y, Chun J, Luster AD. The lysophosphatidic acid receptor LPA1 links pulmonary fibrosis to lung injury by mediating fibroblast recruitment and vascular leak. *Nat Med* 14: 45–54, 2008.
30. Tian B, Lessan K, Kahm J, Kleidon J, Henke C. beta 1 integrin regulates fibroblast viability during collagen matrix contraction through a phosphatidylinositol 3-kinase/Akt/protein kinase B signaling pathway. *J Biol Chem* 277: 24667–24675, 2002.
31. Wallis JM, Borg ZD, Daly AB, Deng B, Ballif BA, Allen GB, Jaworski DM, Weiss DJ. Comparative assessment of detergent-based protocols for mouse lung de-cellularization and re-cellularization. *Tissue Eng Part C Methods* 18: 420–432, 2012.
32. Wang S, Basson MD. Akt directly regulates focal adhesion kinase through association and serine phosphorylation: implication for pressure-induced colon cancer metastasis. *Am J Physiol Cell Physiol* 300: C657–C670, 2011.
33. Weiss DJ. Current status of stem cells and regenerative medicine in lung biology and diseases. *Stem Cells* 32: 16–25, 2014.
34. Wilcox JT, Cadotte D, Fehlings MG. Spinal cord clinical trials and the role for bioengineering. *Neurosci Lett* 519: 93–102, 2012.
35. Xia H, Nho RS, Kahm J, Kleidon J, Henke CA. Focal adhesion kinase is upstream of phosphatidylinositol 3-kinase/Akt in regulating fibroblast survival in response to contraction of type I collagen matrices via a beta 1 integrin viability signaling pathway. *J Biol Chem* 279: 33024–33034, 2004.
36. Xiao L, Du Y, Shen Y, He Y, Zhao H, Li Z. TGF-beta 1 induced fibroblast proliferation is mediated by the FGF-2/ERK pathway. *Front Biosci* 17: 2667–2674, 2012.